# Evaluation of different MRI-based anatomical priors for PET brain imaging

Ameya Atre[1], Kathleen Vunckx[1], Kristof Baete[1], Anthonin Reilhac[2] and Johan Nuyts[1]

***Abstract*—Image reconstruction in emission tomography may benefit from the use of anatomical side information obtained with other imaging modalities in the same subject. One way to implement this, is to use the anatomical image for defining the a-priori distribution in a maximum-a-posteriori reconstruction algorithm. In this contribution, we use the PET-SORTEO Monte Carlo simulator to evaluate three different anatomical priors for PET brain imaging, using MRI for the anatomical image. The priors are: 1) a prior based on a segmentation of the MRI image; 2) the joint entropy prior; 3) a prior (proposed by Bowsher et al. [1]) that encourages smoothness within a position dependent neighborhood, computed from the MRI image. The two latter priors do not rely on an explicit segmentation, which makes them more generally applicable than a segmentation-based prior. The three priors produced a compromise between noise and bias that was significantly better than that obtained with post-smoothed MLEM. The performance of the joint entropy prior was slightly worse than that of the other two priors. In contrast to the joint entropy prior, the Bowsher prior is easily tuned and does not pose convergence problems due to local maxima.**

## I. Introduction

When the finite spatial resolution of the PET system is modelled during maximum likelihood reconstruction, the reconstruction algorithm will automatically apply recovery correction. However, because very high spatial frequencies have been lost during detection, and because high frequencies converge slowlier than low frequencies, this recovery correction is imperfect and produces Gibbs over- and undershoots near edges. The anatomy-based prior can be used to apply smoothing within the tissues but not across the tissue boundaries. This reduces or eliminates the Gibbs over- and undershoots near the tissue boundaries, making the edges steeper and the activity within the different tissues smoother. If there is a strong correspondence between anatomy and tracer uptake (as is usually the case, in particular in brain imaging), then the resulting PET image will have lower noise and improved quantification. The use of a finite resolution model during reconstruction is essential, to ensure that the sharp boundaries promoted by the prior are not in conflict with the smooth boundaries observed in the data.

Many maximum-a-posteriori (MAP) or penalized-likelihood algorithms have been proposed for PET or SPECT reconstruction with anatomical information [2]–[6]. Baete et al [7] evaluated a method called A-MAP, which is based on a segmented MRI image. Such methods produce excellent results if an accurate (and well registered) segmentation is available. Somayajula et al [8] proposed a prior based on mutual information between the PET image and the anatomical image, thus avoiding the need for explicit segmentation. In [9] it was shown that the mutual information based prior may introduce bias, a problem which is avoided by using the joint entropy (JE) instead (i.e. by deleting the marginal entropy term in the mutual information). Bowsher et al [1] proposed a prior which encourages smoothing over an anatomy dependent neighborhood, defined by selecting a set of most similar neighbors in the anatomical image. In this study, three priors are studied: the A-prior used in A-MAP [7], the joint entropy prior [9] and the Bowsher-prior [1]. The priors are evaluated with realistic PET simulations created with the PET-SORTEO Monte Carlo simulator [10], which has been carefully validated [11] and has been used by several other authors. To define the ground truth for the simulated brain images, we used the segmentations from the BrainWeb database at McGill University (Montreal, Canada), [12], [13] to generate realistic software PET brain phantoms. The performance of the priors was assessed using a normal brain phantom and a brain phantom with reduced PET tracer uptake in multiple gray matter lesions, which are not visible in the MRI-image. In these simulations, it was assumed that the registration errors between PET and MRI are negligible, no attempt was done to evaluate robustness in the presence of registration errors, in contrast to the work presented in [4], [14]. We believe this assumption is reasonable for brain imaging with PET $^{18}$F-FDG.

Fig. 1. The phantom. Left column: simulated noise-free MRI-image. Three central columns: the tissue classes for gray matter, white matter and cerebrospinal fluid. Last column: the PET attenuation images.

## II. Methods

### A. Brain images

Figure 1 shows some images from the BrainWeb database, and the attenuation map that was derived from it. The mean image of 27 high resolution T1-weighted gradient-echo MRI scans of the same volunteer has been segmented in many classes, three of which are shown in the figure: gray matter (GM), white matter (WM) and cerebrospinal fluid (CSF). The

[1] Nuclear Medicine, K.U.Leuven, B-3000 Leuven, Belgium, [2] Biospective Inc, Montreal, Quebec, Canada.

This work is supported by SBO grant 060819 “Quantiviam” of IWT and by IAP-grant P6/38 of the Belgian Science Policy.

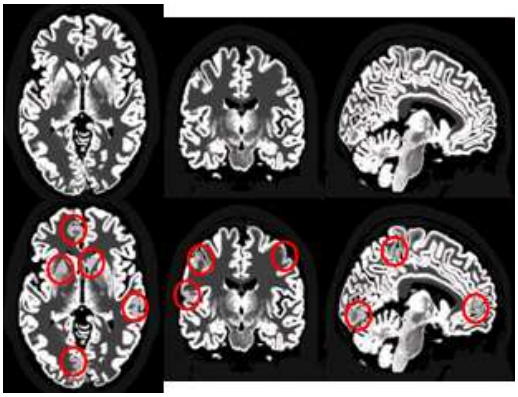

Fig. 2. The simulated brain phantom without and with lesions. The lesions are modeled as a 25% reduction of the tracer uptake in the gray matter, which is enclosed in a 20 mm diameter sphere.

classes also include bone, skin etc, providing at least one label for every voxel in the image. The BrainWeb also provides simulated MRI-scans with or without noise for this software brain phantom. The noise free MRI-image is shown in the figure (left). A PET activity distribution was created by first assigning a single label to each voxel, including labels for combinations of GM and WM, and of GM and CSF. Next, the activity was set to 12500 Bq/ml in GM, 3125 Bq/ml in WM, 0 Bq/ml in air, CSF and bone, and 1000 Bq/ml in all other tissues. Attenuation coefficients were assigned as follows: 0/cm for air, 0.087718/cm for fat, 0.151108/cm for bone, 0.096033/cm for CSF, and 0.098530/cm for brain and all other tissues. The activity and attenuation images were sampled with voxels of $1 \times 1 \times 1$ mm$^3$.

The priors have been evaluated for the normal brain, and for a brain with hypointense gray matter lesions which were invisible to the MRI. Twenty lesions were created by distributing 20 spheres with a diameter of 20 mm in the brain (see Fig. 2). The tracer uptake of the gray matter inside each sphere was reduced with 25%, the activity of the other classes was unaffected. Consequently, the actual volume of the lesion was different in every lesion (ranging from 0.91 to 2.42 cm$^3$), and much smaller than the volume of the sphere.

### *B. Anatomical priors*

The *A-prior* was described previously [7]. It assumes that segmentation images of GM, WM and CSF are available. The segmentation images contain values between 0 and 1, denoting the fraction of the voxel that is occupied by that particular label. In CSF, a Gaussian intensity prior is applied that favors a reconstructed value of zero. Also in WM, a Gaussian intensity prior is applied. However, for WM, the mean WM intensity is not fixed in advance, but estimated during MAP reconstruction. In GM, a smoothing Markov prior is applied; we used the relative difference prior with $\gamma = 0$ [15], which means that there is no increased tolerance for large edges. For voxels containing a mixture of GM and either WM or CSF, it is assumed that the WM or CSF concentration is the same as in pure WM or CSF voxels. Consequently, for those voxels, the MAP algorithm only needs to determine the GM value. In addition, a smoothing Markov prior could be applied to all other tissues. This A-prior was designed for reconstruction of images with normal WM and possible GM lesions. Because the A-prior has a global maximum, the posterior can be optimized with simple gradient ascent algorithms.

The *JE-prior* is obtained by deleting the marginal entropy terms in mutual information, and was found to yield less bias in the reconstructed emission images [9]. In contrast to the A-prior, the joint entropy prior does not need a segmentation, it operates directly on the anatomical image. Because it is computed from the joint histogram, it ignores correlations between neighboring voxels. On the other hand, it has the potential to collect information over large distances, which might be a strength if large organs with uniform tracer uptake are present. It favors piecewise constant images. A problem is that this prior has local maxima: the final reconstruction depends on the initial image and on the optimisation algorithm.

The *Bowsher prior* was proposed in [1]. It is a smoothing Markov prior operating on a position dependent neighborhood. It has the following essential parameters:

1) the definition of a neighborhood $\mathbf{N}$,
2) a similarity metric $S(\alpha_j, \alpha_k)$ for the anatomical image,
3) the number of neighbors $B$ that must be selected for each voxel $j$.

Let $\boldsymbol{\lambda}$ be the PET image with voxel values $\lambda_j, j = 1 \dots J$, and $\boldsymbol{\alpha}$ the registered anatomical image with voxel values $\alpha_j, j = 1 \dots J$. To compute the prior for $\lambda_j$, the neighborhood $\mathbf{N}_j$ of $\alpha_j$ is scanned, computing the similarity metric $S(\alpha_j, \alpha_k), k \in \mathbf{N}_j$. The $B$ voxels with the highest similarity are selected, this set containing these selected voxels is denoted $\mathbf{B}_j$. The smoothing Markov prior in the PET image is then restricted to $\lambda_k, k \in \mathbf{B}_j$. Bowsher et al used the absolute difference to compute the similarity: $S(\alpha_j, \alpha_k) = -|\alpha_j - \alpha_k|$, and considered neighborhoods of different sizes. In this work, we followed the same approach. This method does not rely on a segmentation of the anatomical image. If the Markov prior is based on a convex energy function (as is the case for the quadratic, Huber and relative difference priors), then the Bowsher-prior has a global maximum.

To compute the MAP image, the heuristic but effective gradient ascent algorithm proposed in [15] was used. To accelerate convergence, a scheme with gradually decreasing number of subsets was applied. For the JE-prior, we attempted to avoid convergence to an undesired local maximum by gradually increasing the weight of the prior.

### *C. Parameter tuning*

Each of the priors has several parameters, which should be well tuned for a useful performance comparison. For the tuning, a simple analytical 3D PET simulator was used. This simulator uses a ray tracing projector, which models the resolution by a 3D Gaussian convolution with a full width at half maximum (FWHM) of 4.0 mm in the transaxial planes and a FWHM of 5.45 mm in the axial direction. It also models attenuation, but ignores scatters and randoms. Because the reconstructions used the same projector/backprojector, there

was an exact match of the resolution between simulation and reconstruction.

Two noisy PET acquisitions were simulated, one for the normal brain and one for the brain with the 20 lesions. Both sinograms were reconstructed with the MAP using the different priors and different parameters for each prior. To evaluate the results, a figure of merit $FOM_{GM,N}$ was computed as follows:

$$FOM_{GM,N} = \sqrt{\frac{1}{n_{\text{GM80}}} \sum_{j \in \text{GM80}} \left( \frac{\lambda_j^N - \lambda_j^{N,true}}{\text{GM activity}} \right)^2} \quad (1)$$

where GM80 represents all voxels that belong for more than 80% to the gray matter, $n_{\text{GM80}}$ is the number of elements in GM80, $\lambda_j^N$ is the reconstructed activity in voxel $j$ for the normal brain and $\lambda_j^{N,true}$ is the corresponding true activity, "GM activity" is the true activity in GM. A similar score $FOM_{GM,L}$ is computed for the reconstructions of the brain with lesions. However, $FOM_{GM,N}$ and $FOM_{GM,L}$ are expected to produce very similar values, because the number of lesion voxels is much smaller than the number of normal GM voxels. To assess the quality of the reconstructed lesions, also a contrast is computed:

$$FOM_C = \sqrt{\frac{1}{20} \sum_{l=1}^{20} \left( \frac{(\bar{\lambda}_l^N - \bar{\lambda}_l^L) - (\bar{\lambda}_l^{N,true} - \bar{\lambda}_l^{L,true})}{\text{GM activity}} \right)^2}, \quad (2)$$

where $\bar{\lambda}_l^L$ represents the mean value of lesion $l$ in the reconstruction of the brain with lesions, and $\bar{\lambda}_l^N$ is the corresponding mean value for the reconstruction of the normal brain. The superscript $true$ denotes the corresponding true values. These scores were combined in the final figure of merit that was used for optimizing the parameters:

$$FOM = \sqrt{\frac{FOM_{GM,N}^2 + FOM_{GM,L}^2}{4} + \frac{FOM_C^2}{2}} \quad (3)$$

### D. Realistic simulation

The brain PET-scan was also simulated with the Monte Carlo simulator PET-SORTEO, which takes into account all significant physical effects of the PET acquisition [10], [11]. For this study, a realistic model of the system spatial resolution is required, because the mismatch between the true system resolution and the one used during reconstruction is expected to have a direct impact on the accuracy of the reconstructions. Point source measurements were performed in the Siemens Ecat HR+ scanner of the K.U. Leuven, and simulated with PET-SORTEO. Good agreement was obtained. A result for a point source near the edge of the field of view is shown in Fig. 3. These experiments confirm that the mismatch between the true system resolution and the shift-invariant Gaussian model of the (back)projector is similar for a true PET-system and for PET-SORTEO.

A 30 min $^{18}$F-FDG PET-scan was simulated. The counts in the resulting sinogram were randomly distributed over 30 sinograms. Because the simulated sinogram is subject to Poisson noise (ensured by PET-SORTEO), the 30 sinograms

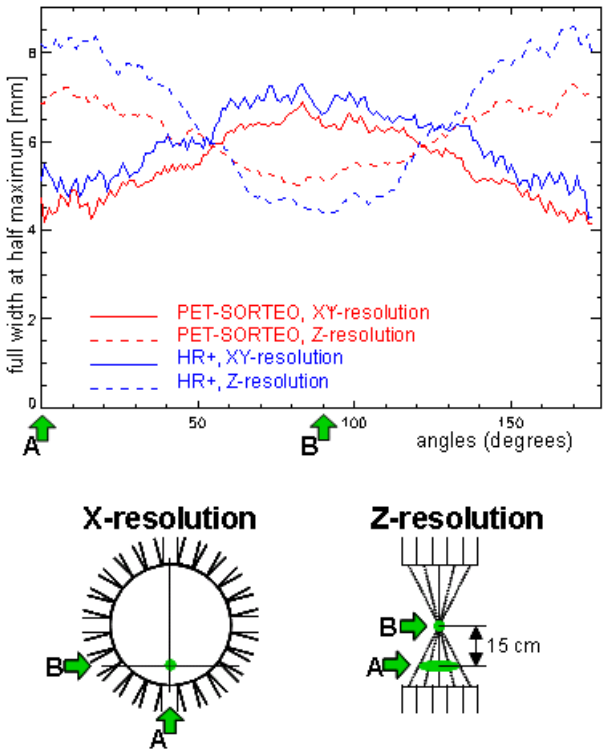


Fig. 3. Sinogram resolution determined with a point source in a real Siemens PET HR+ scanner and in the one simulated by PET Sorteo. The point source is positioned near the edge of the field of view, where the resolution effects are most dramatic.

are independent Poisson realisations of a 1 min brain scan. The final reconstruction images are corrected for the mean decay of $^{18}$F over 30 min.

### E. Reconstruction Parameters

In clinical routine, anatomical information is only used post-reconstruction by inspection of fused (registered) images, e.g. PET and MRI. Hence, post-smoothed maximum-likelihood expectation-maximisation (MLEM) images [17] will be computed to enable comparison with the current image quality. The images were reconstructed with a transaxial pixel size of 2.25 mm and a plane separation of 2.425 mm. To accelerate convergence, ordered subsets (OS) are used with a gradually reduced OS iteration scheme [18]: 10 $\times$ 36, 2 $\times$ 24, 2 $\times$ 16, 2 $\times$ 1 (global iterations $\times$ number of subsets). A 3D isotropic Gaussian smoothing filter with a full width at half maximum (FWHM) varying between 1 and 10 mm, in steps of 1 mm, was applied after reconstruction.

The MAP-reconstructions with anatomical priors used the same iteration scheme. A-MAP was started from a fast MLEM reconstruction image (1 iteration over 36 subsets). A-MAP needs a segmented anatomical image, hence A-MAP-reconstructions were carried out using the known exact segmentation, but also with a segmentation computed with the SPM-software [16] from the simulated noiseless MRI-scan, as well as from a simulated noisy MRI-scan (5% noise calculated relative to the brightest tissue). The parameters to be tuned are

the Markov weights of the priors applied to GM, WM, CSF and other tissues. Also the size of the Markov neighborhood can be changed.

In order to avoid convergence to an undesired local maximum, the JE-reconstruction was initiated with a homogeneous starting image, and the weight of the JE-prior was gradually increased at every full iteration over 36 subsets. For a fair comparison with A-MAP, an extra full iteration over 36 subsets was included in the iteration scheme. The influence on the GM activity and the lesion contrast of different values for the JE-weight, the number of bins for the PET and MRI image (might be different) and the width of the Parzen window to be applied to the PET intensities (see [9]) was evaluated using equation (3).

The Bowsher-reconstruction was started from the same, fast MLEM reconstruction image as A-MAP. Tuning of this algorithm was limited to varying the Markov weight, the size of the neighborhood and the number of selected neighbors. Two neighborhoods were compared, namely a spherical 3×3×3 neighborhood containing 18 possible neighbors, and a spherical 5×5×5 neighborhood with 80 possible neighbors. All neighbors were assigned the same weight, equal to one. Both the JE-prior and Bowsher-prior were computed using the noise-free simulated MRI-scan, and once more using the noisy simulation.

### F. Bias-Noise Analysis

To compare the various reconstruction algorithms, a bias-noise analysis was performed for the reconstructed gray matter activity and for the activity and contrast in the lesion VOIs, based on the reconstruction images of the 30 noisy PET-SORTEO sinograms.

To study the image quality in the GM voxels, the percentage (%) mean absolute bias was calculated, by first averaging the bias in every GM80 voxel over all noisy reconstructions, and next taking the mean over the absolute values of all GM80 voxels:

$$\%\text{mean }|\text{bias}_{GM,N}| = \frac{\frac{100}{{}^{n}\text{GM80}} \sum_{j \in \text{GM80}} \left| \frac{\sum_{n=1}^{30} (\lambda_j^{N,(n)} - \lambda_j^{N,true})}{30} \right|}{\text{GM activity}} \quad (4)$$

with $\lambda_j^{N,(n)}$ the activity in voxel $j$ in the reconstruction image of the $n$-th noisy sinogram of the normal brain, and $|x|$ the absolute value of $x$. The % noise is calculated as:

$$\%\text{noise}_{GM,N} = \frac{100 \sqrt{\frac{\sum_{j \in \text{GM80}} \sum_{n=1}^{30} (\lambda_j^{N,(n)} - \frac{\sum_{n=1}^{30} \lambda_j^{N,(n)}}{30})^2}{29 \cdot J}}}{\text{GM activity}} \quad (5)$$

Similar formulae could be expressed for the brain with lesions.

The % bias and % noise on the activity in the lesion VOIs are defined as:

$$\%\text{bias}_{les,N} = \frac{\frac{1}{30} \sum_{n=1}^{30} \bar{\lambda}_l^{N,(n)} - \bar{\lambda}_l^{N,true}}{\bar{\lambda}_l^{N,true}} \cdot 100 \quad (6)$$

$$\%\text{noise}_{les,N} = \frac{\sqrt{\frac{1}{29} \sum_{n=1}^{30} (\bar{\lambda}_l^{N,(n)} - \frac{1}{30} \sum_{n=1}^{30} \bar{\lambda}_l^{N,(n)})^2}}{\bar{\lambda}_l^{N,true}} 100 \quad (7)$$

for the normal brain reconstructions, and in a similar way for reconstructions of the brain with lesions. The % bias and % noise on the contrast in the lesion VOIs can be calculated by replacing $\bar{\lambda}_l^{N,(n)}$ by $(\bar{\lambda}_l^{N,(n)} - \bar{\lambda}_l^{L,(n)})$ and $\bar{\lambda}_l^{N,true}$ by $(\bar{\lambda}_l^{N,true} - \bar{\lambda}_l^{L,true})$ in expressions (6) and (7).

## III. Results

### A. Reconstruction Images

Based on the $FOM$ of equation (3), the optimal isotropic Gaussian post-smooth filter was found to have a FWHM of 6 mm. Fig. 4(a) and (b) show three orthogonal slices through the unprocessed and 6 mm FWHM post-smoothed MLEM reconstruction image of a PET-SORTEO simulated 1 min FDG PET scan of the brain phantom with 20 lesions, respectively. The former image is very noisy, whereas the latter is fairly smooth.

As expected, very nice images were obtained with A-MAP-reconstruction using the perfect MRI segmentation (Fig. 4(c)). The different tissue classes can clearly be discriminated, because the activity was encouraged to be spread within the tissue classes only. To yield this image, the Markov weights for GM, WM, CSF and other were set to 225, 1000, 1000 and 0. A 3×3×3 Markov neighborhood with 26 neighbors was selected.

Using the JE-prior enhances the visual contrast, detail and quantification of the GM activity compared to post-smoothed MLEM. The white matter suffers from a lumpy activity distribution as the JE-prior tries to explain the noise by assigning small groups of voxels the same activity. During reconstruction, the JE-weight was linearly increased to $35 \times 10^7$. The JE-histogram was computed using 7 bins for the PET image, 25 bins for the MRI image and a Gaussian Parzen window with a standard deviation of 0.9 pixels.

The simulated data were reconstructed with a small and large Bowsher neighborhood. For the former, the 4 most similar (in the MRI) of the 18 neighbors were selected and a Markov weight of 150 was assigned. For the latter, 9 of the 80 neighbors were selected in combination with a Markov weight of 25. Both images show a high level of detail in the GM and a fairly homogeneous activity distribution in WM and CSF. Using a larger neighborhood slightly improves the resolution in the GM. Most lesions in the GM can be discerned from both images. The locations can be verified in Fig. 2 (bottom), because the same slices were selected for visualisation.

### B. Bias-Noise Analysis GM

The unprocessed MLEM image had a relatively high mean absolute bias in the GM voxels (see Fig. 5 (red diamond)), which first decreased and then increased again when applying a post-smooth filter with 1 mm to 6 mm FWHM (green squares). The noise reduced from 95% to 14%.

The A-MAP-reconstruction based on perfectly segmented MRI data (black plusses) has low mean |bias| and slightly lower noise than post-smoothed MLEM. However, using imperfect (SPM) segmentation data doubled the mean |bias| and quadrupled the noise (black stars). The JE-prior (pink plusses) performs slightly worse than the ideal A-prior reconstruction.

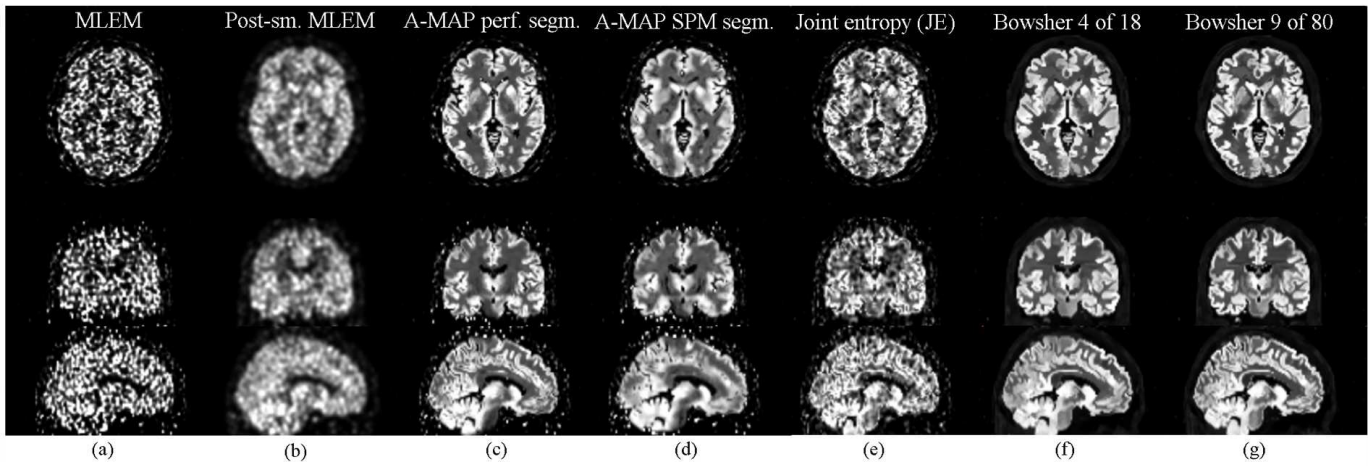


Fig. 4. Example reconstruction images of a PET-SORTEO simulated 1-min FDG-PET scan of a brain with hypointense lesions using the simulated noiseless MRI. The following reconstruction algorithms were used: (a) MLEM, (b) post-smoothed MLEM (6 mm FWHM), (c) A-MAP using perfectly segmented MRI information, (d) A-MAP using SPM segmented MRI information, (e) joint entropy, (f) Bowsher using 4 out of 18 neighbors, and (g) Bowsher using 9 out of 80 neighbors.

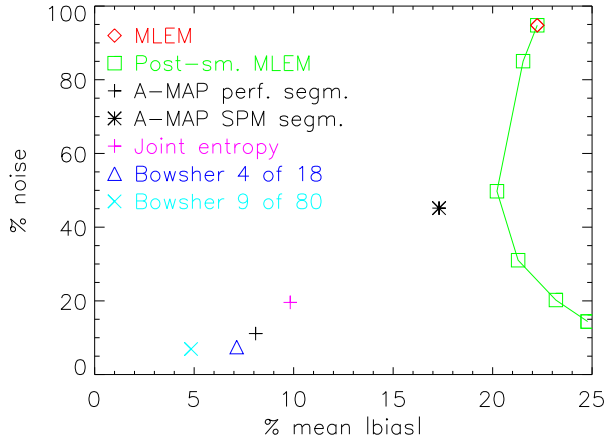


Fig. 5. Bias-noise analysis of the activity in the GM voxels of the normal brain. The percentage mean absolute bias is plotted with respect to the percentage noise for the different tested reconstruction algorithms.

In comparison with post-smoothed MLEM, it reduced the mean |bias| by 60% at the cost of a bit more noise. Both Bowsher-priors (dark blue triangles and light blue crosses) slightly outperform the ideal A-prior reconstruction. The larger neighborhood further reduced the mean |bias| (light blue crosses). All evaluated anatomical priors yielded a decrease in mean |bias| in the GM. Most of them also reached a similar or even lower noise level, except for the A-prior using SPM segmentation.

Fig. 5 shows the results for the normal brain, but those for the brain with lesions are almost identical. Also the results obtained from using noisy MRI data were very similar (not shown).

### C. Bias-Noise Analysis Lesion VOIs

In Fig. 6, the % noise in the lesion VOIs is plotted with respect to the % bias for (a) the normal brain and (b) the brain with lesions. The symbols depict the mean value averaged over the 20 lesions. The bars indicate +/- 1 standard deviation, to illustrate the variation over the lesions. The dashed vertical line denotes zero bias.

From these results, it shows that MLEM (red diamonds) suffers from the highest noise level in the lesions. The anatomical priors all approach the low noise level of 6 mm FWHM post-smoothed MLEM (green squares). The noise behaviour is very similar in the lesion VOIs of the normal brain and those of the brain with lesions.

The bias behaves somewhat differently in the two phantom images, when using an anatomical prior. For MLEM, a negative bias is observed for both images, and post-smoothing introduced extra bias. However, A-MAP with perfect segmentated MRI data (black plusses), JE (pink plusses) and both Bowsher reconstructions (dark blue triangles and light blue crosses) have very limited negative bias in the normal brain and small to moderate positive bias in the brain with lesions, indicating that some of the surrounding GM activity is smoothed into the lesion VOIs. The JE and the Bowsher reconstruction using the large neighborhood suffer most from positive bias. A-MAP using SPM segmented MRI data has somewhat less negative bias than unprocessed MLEM in both cases.

### D. Bias-Noise Analysis Lesion Contrast

Fig. 6(c) shows the bias-noise plot for the contrast in the lesion VOIs. We defined the contrast in a lesion VOI as the difference between the mean activities in that VOI in the normal brain image and in the brain image with lesions. The trends in the noise behaviour of the various algorithms are similar to those observed in the lesion VOIs in the separate images (Fig. 6(a) and (b)). MLEM has the highest noise level (red diamond), which is strongly reduced by the post-smoothing filter (green square). Again, the noise on the contrast in the lesion VOIs is only slightly higher when using an anatomical prior for regularisation instead of a post-smoothing filter.

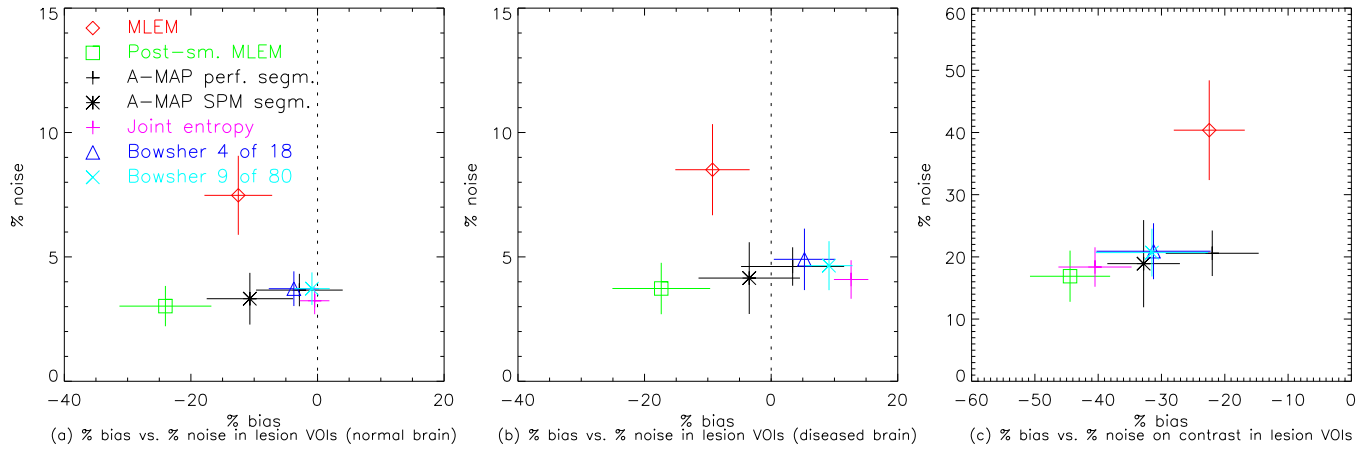


Fig. 6. Bias-noise analysis of the activity in the lesion VOIs (a) in the normal brain and (b) in the brain with lesions, and of the contrast in the lesion VOIs (c). The percentage bias is plotted with respect to the percentage noise for the different tested reconstruction algorithms.

MLEM (red diamond) and A-MAP using perfectly segmented MRI data (black plus) yield the lowest bias on the contrast, whereas post-smoothed MLEM almost halves the contrast. JE-reconstruction (pink plus) also loses a big share of the contrast. The two Bowsher priors and the A-prior using an SPM segmentation perform intermediately in terms of bias.

Both the bias-noise results for the lesion VOIs and for the lesion contrast were very similar when using the noisy instead of the noiseless MRI data. Therefore, the plots were omitted here.

## IV. Discussion

In these simulations, we have assumed that the registration errors are negligible, which is a reasonable assumption for rigid registration of FDG PET and MRI in brain imaging. The reconstruction uses a shift invariant resolution model, while the PET-SORTEO simulator produces a realistic shift variant resolution as illustrated in Fig. 3. For A-MAP, realistic segmentation errors were obtained by segmenting the simulated MRI image with the SPM software package. For these reasons, we believe that the results of this study are clinically relevant.

As illustrated in Fig. 5, the anatomical priors yield an excellent reconstruction of the gray matter, with a bias-noise performance clearly superior to that of post-smoothed MLEM-reconstruction. In the normal image, there is a perfect match between gray matter activity and anatomy. Consequently, by further increasing the weights of the prior, bias and noise can probably be further decreased in Fig. 5. However, this would result in a poorer reconstruction of the cold gray matter lesions in the diseased brain. These cold lesions are invisible in the anatomical image, and with increased weight of the priors, there will be increased smoothing over the lesion boundary within the gray matter.

The reconstruction image quality of the lesions can best be appreciated in Fig. 6(c), which shows the difference in mean reconstructed lesion value between normal and diseased brain, averaged over the 20 lesions. A-MAP with ideal segmentation outperformed the other methods. However, when a realistic, imperfect segmentation is used, Fig. 5 and 6(c) indicate that the Bowsher-prior can outperform A-MAP.

The Bowsher-prior also produced a better lesion contrast than the joint entropy prior. This is probably because the Bowsher prior operates locally, while the joint entropy prior operates on all image intensities simultaneously, disregarding their positional information. The moderate decrease of 25% in the lesions turned out to be very challenging for the joint entropy prior, because this decrease was similar to the amplitude of the noise in the GM voxels. We were unable to find a combination of parameters (number of bins, width of the Parzen window, weight of the prior) that produced a better contrast than the one shown in Fig. 6(c). If the number of histogram bins was increased to obtain a better lesion contrast, noise propagation deteriorated, because the prior then accepted the noise as small isolated clusters in the joint histogram. An additional problem of the joint entropy prior is the presence of local maxima. For this brain image, the best results were obtained by starting the iterations from a uniform image, rather than from an MLEM-reconstruction, and by gradually increasing the weight of the prior.

In contrast to the joint entropy prior, the Bowsher prior behaves more predictably, and its parameters are more easily tuned. In addition, because this prior yields a unique maximum for the objective function, convergence is not a problem. Consequently, we will further study this prior for clinical applications.

## V. Conclusion

Three anatomical priors were evaluated in a realistic simulation of PET brain imaging with FDG, coregistrered to MRI. All three priors outperformed post-smoothed MLEM. The prior previously proposed by Bowsher et al seems to have the best potential for this clinical application.

## References

[1] JE Bowsher, H Yuan, LW Hedlund et al., TG Turkington, G Akabani, A Badea, WC Kurylo, CT Wheeler, GP Cofer, MW Dewhirst, GA Johnson, “Using MRI information to estimate F18-FDG distributions in rat flank tumors”, *IEEE Nucl Sci Symp Conf Record*, 2004, pp 2488-2492.

[2] B Lipinski, H Herzog, E Rota Kops et al., Oberschelp, HW Müller-Gärtner, “Expectation maximization reconstruction of positron emission tomography images using anatomical magnetic resonance information”, *IEEE Trans Med Imaging*, vol. 16, no. 2, pp. 129-136, 1997.

[3] A Rangarajan, IT Hsiao, G Gindi, “A Bayesian joint mixture framework for the integration of anatomical information in functional image reconstruction”, *J Math Imaging Vision*, vol 12, pp 199-217, 2000.

[4] C Comtat, PE Kinahan, JA Fessler et al., “Clinically feasible reconstruction of 3D whole-body PET/CT data using blurred anatomical labels”, *Phys Med Biol* vol 47 pp 1-20, 2002

[5] S Kulkarni, P Khurd, I Hsiao, et al., “A channelized Hotelling observer study of lesion detection in SPECT MAP reconstruction using anatomical priors”, *Phys Med Biol* vol 52, pp 3601-3617, 2007

[6] X Ouyang, WH Wong, VE Johnson, X Hu, Chin-Tu Chen, “Incorporation of correlated structural images in PET image reconstruction”, *IEEE Trans Med Imaging* 1994; 13: 627-640.

[7] K Baete, J Nuyts, K Van Laere et al., W Van Paesschen, S Ceyssens, L De Ceuninck, O Gheysens, A Kelles, J Van den Eynden, P Suetens, P Dupont. “Evaluation of anatomy based reconstruction for partial volume correction in brain FDG-PET”, *NeuroImage*, vol 23, pp 305-317.

[8] S Somayajula, E Asma, RM Leahy, “PET image reconstruction using anatomical information through mutual information based priors”, *Conf. Record: IEEE Nucl Sci Symp Med Imag Conf* , Puerto Rico, pp 2722-2726, 2005.

[9] J Nuyts. ”The Use of Mutual Information and Joint Entropy for Anatomical Priors in Emission Tomography”. *IEEE Nucl Sci Symp Conf Record*, 2007, pp 4149 - 4154

[10] A Reilhac, C Lartizien, N Costes et al. “PET-SORTEO: A Monte Carlo-based simulator with high count rate capabilities”, *IEEE Trans Nucl Sci.*, 2004; 51 (1): 46-52.

[11] A Reilhac, “Validation et exploitation d’un simulateur TEP de Monte Carlo”, PhD-thesis, Institut National des Sciences Appliques de Lyon, 2007.

[12] website: “http://www.bic.mni.mcgill.ca/brainweb/”.

[13] DL Collins, AP Zijdenbos, V Kollokian, JG Sled, NJ Kabani, CJ Holmes, AC Evanset. “Design and construction of a realistic digital brain phantom”, *IEEE Trans. Med. Imaging*, 1998; 17: 463-468.

[14] J Cheng-Liao, J Qi. “PET image reconstruction with incomplete anatomical edge information using level set method” IEEE NSS MIC, Orlando, 2009: M03-5.

[15] J Nuyts, D Bequé, P Dupont, et al “A concave prior penalizing relative differences for maximum-a-posteriori reconstruction in emission tomography”, *IEEE Trans Nucl Sci*, vol 49, pp 56-60, 2002.

[16] Software package, Wellcome department of cognitive neurology (London, UK), http://www.fil.ion.ucl.ac.uk/spm

[17] L. S. Shepp and Y. Vardi, “Maximum likelihood reconstruction for emission tomography.” *IEEE Trans. Med. Imag.*, vol. MI-1, pp. 113-122, 1982.

[18] M. H. Hudson and R. S. Larkin, ”Accelerated image reconstruction using ordered subsets of projection data.” *IEEE Trans. Med. Imag.*, vol. 13(4), pp. 601-609, 1994.